Soft Pneumatic Artificial Muscles with Low Threshold Pressures for a Cardiac Compression Device

by

Steven Obiajulu

Submitted to the
Department of Mechanical Engineering
in Partial Fulfillment of the Requirements for the Degree of

Bachelor of Science in Mechanical Engineering

at the

Massachusetts Institute of Technology

June 2013

Signature of Author: _____
Department of Mechanical Engineering
May 8, 2013

Certified by: _____
Daniel D. Frey
Professor of Mechanical Engineering and Engineering Systems
Thesis Supervisor

Accepted by: _____
Anette Hosoi
Associate Professor of Mechanical Engineering
Undergraduate Officer

Soft Pneumatic Artificial Muscles with Low Threshold Pressures for a Cardiac Compression Device

by

Steven C. Obiajulu

Submitted to the Department of Mechanical Engineering
on May 8, 2013 in Partial Fulfillment of the
Requirements for the Degree of

Bachelor of Science in Mechanical Engineering

ABSTRACT

In this paper, I present the design, fabrication and characterization of fully soft pneumatic artificial muscles (PAMs) with low threshold pressures that are intended for direct cardiac compression (DCC). McKibben type PAMs typically have a threshold pressure of at least 100kPa and require rigid end fittings which may damage soft tissue and cause local stress concentrations, and thus failure points in the actuator. The actuator design I present is a variant on the McKibben PAM with the following key differences: the nylon mesh is embedded in the elastomeric tube, and closure of the end of the tube is achieved without rigid ends. The actuators were tested to investigate the effects of mesh geometry and elastomer material on force output, contraction, and rise time. Lower initial braid angles and softer elastomer materials provided the best force, contraction, and rise times; Up to 50N of force, 24% contraction, and response times of 0.05s were achieved at 100kPa. The actuators exhibited low threshold pressures (<5kPa) and high rupture pressures (138kPa - 720kPa) which suggest safe operation for the DCC application. These results demonstrate that the actuators can achieve forces, displacements, and rise times suitable to assist with cardiac function.

Thesis Supervisor: Daniel D. Frey
Tile: Professor of Mechanical Engineering and Engineering Systems

ACKNOWLEDGMENTS

I would like to thank Dr. Frank Pigula for providing insight into the clinical problem and for proposing the use of pneumatic artificial muscles in direct cardiac compression. I would like to thank Ellen Roche for help with experimental characterization of the actuators and for help fabricating the mesh-based prototype. I would like to thank Prof. Conor Walsh for allowing me to use his laboratory for the research. I would like to acknowledge the Wyss Institute for Biologically Inspired Engineering for funding this research and Ramses Martinez, Michael Wehner, and Kevin Galloway for providing input on fabrication methods for soft actuators and methods for their experimental characterization.

TABLE OF CONTENTS

List of Figures

List of Tables

1 INTRODUCTION

Pneumatic artificial muscles (PAMs) are actuators that contract when pressurized with air. The most widely used PAM is the Mckibben PAM (Daerden & Lefeber, 2002). This tube-like actuator was developed in the 1950s for actuating orthotics because of the similarity between its load-length curve and that of skeletal muscle. McKibben PAMs consist of a rubber tube enclosed in a textile mesh or braid. The mesh contracts axially when the bladder expands it radially, acting in a manner similar to a scissor linkage. At their ends, the bladder and mesh are crimped together to allow mechanical coupling to a load.

McKibben PAMs have been used in a wide range of applications including robotics, orthotics, and industrial automation (Andrikopoulos, Nikolakopoulos, & Manesis, 2011). One potential new application is in direct cardiac compression (DCC), a treatment for end-stage heart failure. DCC involves implantation of a device that surrounds the heart and contracts in phase with the native heartbeat to provide direct mechanical assistance during the ejection phase (systole) of the cardiac cycle. Unlike other treatment options, DCC does not require contact with the patient's circulating blood. This is advantageous because blood-contacting devices are associated with thromboembolic events, hemolysis, immune reactions and infections (Oz, Artrip, & Burkhoff, 2002). DCC devices are typically implanted through open heart surgery and are usually powered through a transcutaneous drive line. A number of actuation strategies for DCC have been implemented, pneumatic and otherwise (Kung & Rosenberg, 1999; Ming et al., 2005; Moreno et al., 2011a, 2011b; Shahinpoor & Kim, 2001; Shahinpoor, 2010; Shiraishi et al., 2005; Trumble, Park, & Magovern, 1999), but to date it seems that McKibben PAMs have been ignored as an actuation strategy. If integrated into DCC devices, McKibben PAMs may provide a more physiological and atraumatic actuation strategy because they have load-length curves

similar to human muscle (Chou & Hannaford, 1994; Klute, Czerniecki, & Hannaford, 1999) and are self-limiting.

Unfortunately, traditional McKibben PAMs have properties that could limit their use inside the human body. The foremost drawback is that McKibben PAMs typically have a threshold pressure of 100kPa due to friction between the bladder and mesh coupled with an initial lack of contact between the walls of the bladder and mesh. This limitation prevents precise control of force and displacement. Low forces and controlled displacements cannot be achieved with PAMs that have high threshold pressures because there is a rapid jump in force and displacement as the threshold is passed(Daerden & Lefeber, 2002). This may be traumatic to the heart after many cycles. Besides that effect, a higher threshold pressure would require a higher operating pressure, but it is unsafe to have high pressures inside the body in case the device ruptures. Finally, a high threshold pressure introduces a delay since the actuator cannot begin delivering power until the threshold is passed.

Additionally, most existing McKibben PAMs have rigid attachment points at their ends that allow for easy mechanical coupling to a load. If McKibben PAMs were used for DCC, such features might damage a patient's soft tissue. Also, the crimps have been shown to cause early fatigue failure due to introduction of stress concentrations (Daerden & Lefeber, 2002; Woods, Gentry, Kothera, & Wereley, 2012).

In the present study, a new variant of the McKibben PAM that integrates the braid with an elastomeric tube was designed to be compatible with DCC. The PAMs were designed with a low threshold pressure and soft ends. Soft attachment methods were also developed and tested. The PAMs were evaluated to assess whether they provided suitable force, contraction, and rise times

for direct cardiac compression and to evaluate how output force and contraction were affected by changes to elastomeric material and braid angle. Finally two integrated prototypes were fabricated for future animal testing.

2 BACKGROUND

2.1 Medical problem

Heart Failure (HF) occurs when a patient's heart can no longer supply sufficient blood flow to the body. The decreased cardiac output usually leads to progressive failure of internal organs and a shortened lifespan. Heart failure is the possible result of a number of chronic heart diseases such as coronary artery disease, hypertension, arrhythmia, heart attack and congenital defects; In the United States, the lifetime risk of developing heart failure is roughly 20% and at any time about 2.2% of the adult population suffers from heart failure (A. Mosterd & Hoes, 2007).

Heart failure can be caused by insufficient contraction of the heart or insufficient filling. In roughly two thirds of heart failure cases, the condition is attributed to insufficient contraction of the left ventricle, the largest chamber of the heart (Vasan, Benjamin, & Levy, 1995). Heart failure is commonly identified by the ejection fraction of a patient's left ventricle, the ratio of blood ejected from the left ventricle per stroke to volume of the left ventricle. Heart failure is usually defined as a left ventricular ejection fraction (LVEF) of $\leq 40\%$.

Currently, the preferred method for increasing ejection fraction is heart transplantation; however, the demand for transplants greatly exceeds the supply, and demand is growing. Blood contacting devices like ventricular assist devices (VADs) and total artificial hearts are another viable treatment option, but due to interactions with the patients' blood, they cause blood clotting and greatly increase the risk of stroke in patients. In fact, blood clots are the leading cause of

death in patients on VADs (Shahinpoor, 2010). To address the shortcomings of blood contacting assist devices, a number of non-blood contacting devices are currently under development (Alazmani et al., 2012; Kung & Rosenberg, 1999; Moreno et al., 2011b; Oz et al., 2002) although none have received FDA approval yet.

2.2 Extracardiac Compression Devices Prior Art

Extracardiac compression, also known as direct cardiac compression (DCC), is a non-blood contacting method of cardiac assistance for treating heart failure. No extracardiac compression device has been approved for commercial use in humans to date, but extracardiac compression is currently a subject of medical research(Oz et al., 2002). Extracardiac compression was first proposed by Anstadt et al in 1965. Anstadt was most likely inspired by dynamic cardiomyoplasty, a heart failure treatment wherein skeletal muscle is wrapped around the heart and contracted with the heart to boost cardiac output. Anstadt's device, commonly referred to as the Anstadt cup, was designed for resuscitation and short term (< 5 days) support of a totally arrested heart. The device consisted of an inflatable rubber membrane with an inextensible outer wall. When the inner membrane was inflated, the heart was compressed while the inextensible outer wall prevented unwanted expansion against other organs around the heart. A figure of the Anstadt cup around a heart is shown in Figure 2.1.

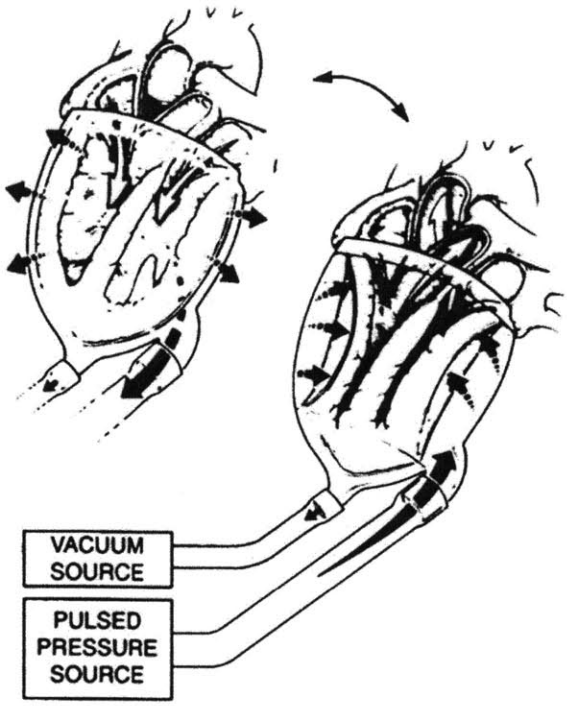

Figure 2.1: A figure showing the Anstadt cup around a heart (Anstadt et al., n.d.). The image on the left shows the heart during expansion (diastole) and the image on the right shows the heart during compression (systole).

The device was designed to be capable of rapid implantation in an emergency setting. Both sides of the heart were compressed at once to assist the left and right ventricles. Continuous suction was used to secure the cup on the heart. This suction also allowed the Anstadt cup to not only compress the heart, but to expand it as well to aid cardiac filling. The original device was not paced with the heart because it was removed once the heart returned to perfusing rhythm.

In 2000, Cardio Technologies Inc (Pine Brook, NJ) developed a cup-shaped cardiac assist device similar to the Anstadt cup called the CardioSupport System (Figure 2.2). The device is pneumatic and has an inner cuff which inflates to compress the heart. Like the Anstadt cup, the device is designed to be implanted quickly for short term support for acutely failing hearts. The device is also designed to be removed shortly after the failing heart recovers. Unlike the Anstadt

cup, the device is customized to size of patient's heart and can be synchronized with the native heart using ECG leads implanted in the cup. A computer console can be used to adjust the parameters of the cardiac assistance like and frequency of cuff inflation (Oz et al., 2002).

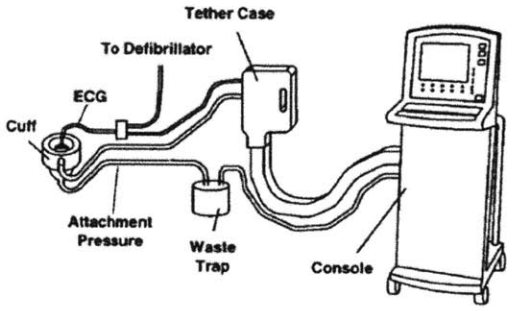

Figure 2.2: A schematic of the CardioSupport System (Oz et al., 2002). The device consists of an inflatable cuff that fits around the heart in phase with the native heart beat using ECG for pacing. A computer console can be used to change the parameters of the contraction.

The Heart Booster, created by AbioMed Inc (Danvers, MA) is another extracardiac compression device that compresses the heart by contracting to a smaller radius, not by expanding radially. The device is run at much higher pressure than delivered to heart, but as a result, pumps a greater volume of blood for each volume of fluid pumped into the device. The device was designed to operate with low volumes because the device was intended to be a fully implantable device. Unlike the previous devices, it was designed for long term support rather than acute interventions(Kung & Rosenberg, 1999).

Smooth outer surfaces and a proprietary polymer are used to prevent tissue ingrowth during the long term use. The device was designed to be implanted minimally invasively (through a mini thoracotomy) and anchored to the pericardium attachment, but this attachment method is prone to creep in the long term. In an in vitro model, the device must be operated at about 100

kPa for physiological blood flow rates at a physiological afterload (6L/min at 115torr) (Kung & Rosenberg, 1999).

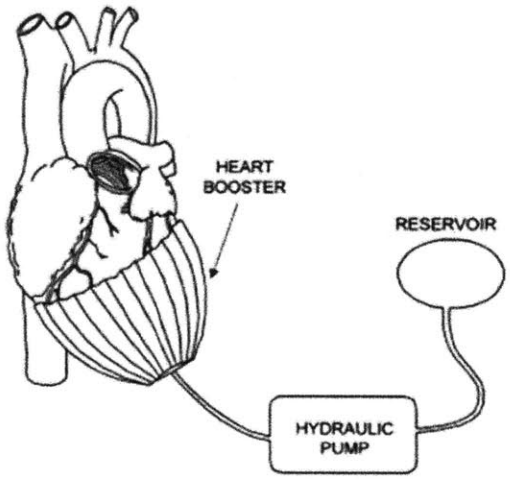

Figure 2.3: A schematic of the Heart Booster cardiac assist device (Kung & Rosenberg, 1999).

Another recently developed DCC device is the HeartPatch (Heart Assist Technologies Pty Ltd; St Leonards, Australia), a device composed of two inflatable patches that are placed over the right and left ventricle to allow independent actuation of the ventricles (Figure 2.4). The device uses patches to provide "non-surround" cardiac assistance because DCC devices that completely surround the heart have been shown to impede ventricular filling and reduce cardiac output(Mau, Menzie, Huang, Ward, & Hunyor, 2011). Another key feature of the device is that the ventricles are actuated independently, meaning different pressures can be delivered to each ventricle. This is especially important since the left ventricle requires more compression since it operates at a significantly higher pressure than the right ventricle. This difference in pressure is because the left ventricle supplies the entire body with blood, whereas the right ventricle only pumps blood through the lungs for oxygenation.

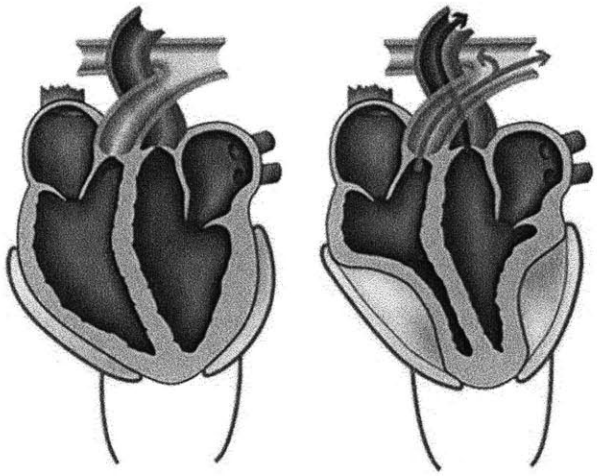

Figure 2.4: The Heart Patch device provides biventricular cardiac assistance that does not constrain ventricular filling (Mau et al., 2011).

The Heart Patch device can be delivered minimally invasively and is left in place for two weeks before initiating cardiac compression so that biointegration can occur to hold the patches in place. Since the device relies on biointegration, it cannot provide immediate cardiac assistance in an emergency setting like the Anstadt Cup or CardioSupport System. Instead, this device is intended for chronic use like the Heart Booster.

One shortcoming of the Heart Patch is that the action of the Heart Patch produces tensile peel stresses at its edges because as the center of the patch inflates and compresses the ventricle, the edges are pulled away from the ventricle. After repeated actuation, the peel stresses can cause delamination of the edges of the patch (Huang & Hunyor, 2004). Delamination would reduce the viability of the Heart Patch for chronic use. The Heart Patch device also creates unnatural deformation of the underlying ventricle because the device inverts the curvature of the ventricular wall. Heart valves are quite sensitive to distortion of the ventricular walls and distortions may lead to impaired valve closure and subsequent valve leakage (Melvin, 2006).

3 DESIGN OF PNEUMATIC ARTIFICIAL MUSCLES

3.1 Overview of Pneumatic Artificial Muscles

Pneumatic Artificial Muscles (PAMs) are actuators that contract axially when pressurized with air. The most commonly used PAM, the McKibben actuator, consists of an elastomeric bladder inside a mesh sleeve. When the bladder expands the mesh radially, the mesh contracts axially. The force produced by this axial contraction increases linearly with increasing internal pressure and decreases with increasing percent contraction. Using energy conservation, an expression for the force output of a PAM can be derived. The relevant parameters are defined in Figure 3.1.

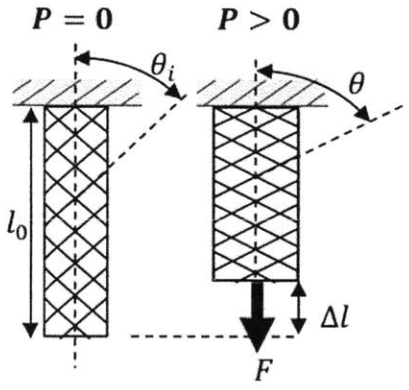

Figure 3.1: Definition of parameters of geometric model of a Mckibben PAM.

The energy conservation equation for a PAM undergoing infinitesimal contraction, dl, is given by

$$-F \cdot dl = P \cdot dV, \qquad (1.1)$$

where F is output force, P is input pressure, and dV is change in the actuator's internal volume. Rearranging Eqn. 1.1 yields

$$F = -P\frac{dV}{dl}. \qquad (1.2)$$

This equation applies to a wide range of pneumatic actuators including pistons, for which *dV/dl* would simply reduce to the area of the piston, yielding the familiar expression *F=P*A*. For PAMs, however, *dV/dl* is not constant because volume is not linearly related to actuator length. The mesh used to constrain the bladder of a PAM defines the *dV/dl* function for that particular PAM. Using a simple kinematic model of a cylindrical uniform braid with braid angle θ, Schulte was able to find an expression for *dV/dl* for a mesh-constrained PAM. Inserting his expression for *dV/dl* into Eqn 1.2 yields (Schulte, 1961)

$$F = P \cdot \frac{\pi D_0^2}{4}(3\cos^2\theta - 1), \qquad (2)$$

where D_0 is the diameter of the mesh at a braid angle of 90 degrees.

Contraction, ϵ of a McKibben actuator is defined as

$$\epsilon = \frac{l_0 - l}{l_0}, \qquad (3)$$

where l is length and l_0 is initial length. Assuming Schulte's simple geometric model of a PAM, the relation between contraction and braid angle is (Tondu, 2012)

$$\epsilon = 1 - \frac{\cos(\theta)}{\cos(\theta_0)}. \qquad (4)$$

In the above equation, the initial braid angle, θ_0, is a constant determined by the braid pattern used to construct a PAM. Increasing pressure drives the braid angle asymptotically to θ_{max} which is about 54.7° because internal volume is maximized at this angle (Horn & Kuipers, 1988; Tondu, 2012). Since increasing pressure drives θ to θ_{max} and θ_0 is assumed to be fixed for a

PAM, Eqn. 4 implies that increasing pressure drives contraction to a constant value. One implication of this result is that the capacity for contraction can be increased only by lowering θ_0.

Another implication is that if $\theta_0 = \theta_{max}$, no axial contraction occurs. For all PAMs, radial expansion accompanies axial contraction, but radial expansion of the ends of the actuator can cause the air supply line to be ejected. To prevent this from happening, rigid end fittings are typically used to secure the air supply line. In the PAMs developed here, instead of using rigid ends fittings, θ_0 was locally set close to θ_{max} at the ends of the mesh to prevent radial expansion there. Since the braid angle was only modified over a small length of the PAM, the effect on overall force output and contraction was assumed to be negligible.

3.2 Force, Contraction, and Rise Time Requirements

The force requirements of the actuators for the DCC device can be estimated using a simple model of a hemispherical DCC device cupped around the bottom of a spherical heart as shown in Figure 3.2.

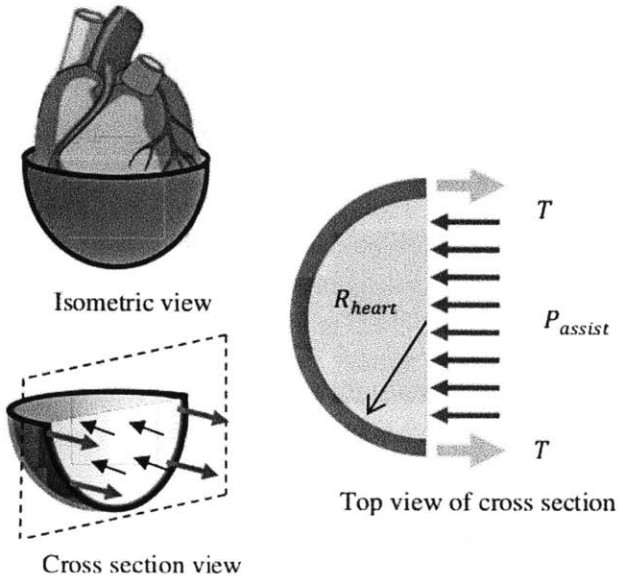

Figure 3.2: An idealized model of a cup-shaped DCC device that sits over the apex of the heart and a free body diagram of half of the DCC device.

In this simple, idealized model, the force from the PAM creates the tension, *T*. The free body diagram of a cross section passing through the center of the model DCC device is also shown in Figure 3.2. If the device and the heart are in equilibrium, the tension required to apply the pressure P_{assist} to the heart is

$$T = \frac{P_{assist} \cdot A_x}{2}, \tag{5}$$

where A_x is the projected cross-sectional area of the device. In a study using a cup-shaped pneumatic DCC device similar to the idealized model in Figure 3.2, an assistance pressure of 140mmHg (18.7kPa) was needed to restore pumping function to a totally arrested (no native cardiac function) canine heart (Anstadt et al., n.d.). Using the above hemispherical cup model and assuming a diameter equal to a typical transverse heart diameter in adult males

(13cm)(Oberman, Myers, Karunas, & Epstein, 1967), this pressure would correspond to a required tensile force of approximately 60N. Alternatively, in cases where native cardiac function is impaired but not totally stopped, lower assistance pressures are required to raise cardiac output to normal levels. For example, an assistance pressure of 20mmHg (2.7kPa) applied using a cup-shaped assist device has been shown to significantly increase the ejection fraction of failing hearts in live sheep (Carrington & Huang, 2003). This assistance pressure roughly corresponds to a tension of only 10N using Eqn 5. These first order estimates suggest that a tension roughly in the range of 10N to 60N is suitable for DCC. In the envisioned DCC device, the total wall tension would be produced by multiple PAMs placed in the wall of the device in a transverse orientation. Actuation with more PAMs in parallel allows the force to be more distributed and perhaps gentler on the heart. To enable the use of more actuators in parallel, the diameter of the actuators was designed to be as small as was feasible with the fabrication techniques available.

Required contraction can be estimated using the measure of cardiac function called fractional shortening (FS). FS is a measure of the percent change in the length of a cardiac dimension between diastole (expansion) and systole (contraction). In cases of left ventricular dysfunction, FS is less than or equal to 25% (a Mosterd et al., 1999). The actuators developed here must provide similar or better percent contraction to be useful in DCC.

The response time of a direct cardiac compression device must be similar to the contraction time of the human heart. Systole occurs in about 0.3 seconds in humans, so rise times much less than 0.3s are desired in order to keep pace with the heart. If the contraction time of a DCC device were much longer than systole, filling of the heart's ventricles, which occurs after systole, could be impeded (Walker et al., n.d.). The Functional requirements are summarized in Table 3.1.

Table 3.1: Functional requirements for actuators for DCC device

Functional Requirement	Criteria
Force	10 N- 60 N
Contraction	~25%
Rise Time	<0.3 s

4 FABRICATION OF PNEUMATIC ARTIFICIAL MUSCLES

The fabrication procedure for the PAMs consisted of molding elastomeric tubing, preparing a mesh, bonding the mesh to the tubing, and then sealing the ends. Elastomeric tubing was molded in house using a low stiffness elastomer (Shore OO-30, Ecoflex 00-30, Smooth-on, Inc.) or higher stiffness elastomer (Shore A-28, Elastosil M4601, Wacker Chemie AG). To create the tubing, the mixed prepolymer was poured into a plastic mold and degassed in a vacuum chamber at 10kPa absolute pressure for 10 minutes. Afterwards, the elastomer was cured for 1 hour in a pressure chamber heated to 60°C. To enable the use of more actuators in parallel, the diameter of the tubing was made as small as possible. A minimum outer diameter of 8mm and wall thickness of 2mm was chosen because molds for narrower tubing were difficult to fill using gravity alone.

4.1 Mesh modification

Before being molded over the elastomeric tubing, the mesh was locally modified to resist expansion at its ends and to prevent fraying. This was achieved by locally heating the mesh (expandable sleeving, Techflex, Inc.) and increasing the braid angle. Figure 3a shows the process diagram. The mesh was placed over a steel rod for support and the region of the tube that was not

being modified was covered with heat shrink to maintain the orientation of the fibers underneath. The end of the mesh sleeve was held to the rod with a ring of heat shrink tubing to prevent fraying when the ends were heated and compressed. The exposed mesh sleeve was compressed by sliding the two heat shrink protected areas together. When the exposed mesh was compressed, it bulged to a larger diameter, but collapsed back to the diameter of the rod when heated. After the new configuration was achieved, the fibers were allowed to cool to lock the new shape into place. To verify that the braid angle was close to the neutral angle, manual expansion of the mesh was attempted and the resistance to expansion was assessed qualitatively. A mesh that was modified using the above procedure is shown in Fig. 3b.

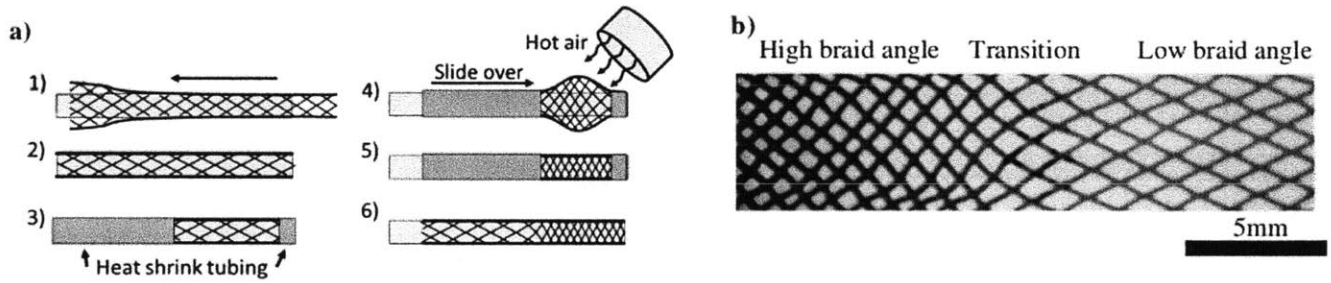

Figure 4.1: A) The process diagram for varying the mesh braid angle. B) Microscope image of a modified braid.

Different global braid angles were achieved by using different meshes between actuators or by using the same mesh and slightly changing the diameter of the actuator because diameter and braid angle are coupled. Since the braids were not made in-house, differences in mesh construction besides braid angle, like weave density, could not be controlled for. The braid angle of each actuator was estimated using a microscope and the measurements for the actuators is given in Table 4.1.

Table 4.1. Braid measurements.

Mean θi (deg)	St Dev. (deg)	Initial diameter (mm)
22.6	0.8	8
28.6	0.7	8
31.7	1.1	8
39.5	1.6	10
45.1	0.5	12

4.2 Bonding of Mesh to Elastomeric Tube and Molding Ends

Once the mesh was prepared, it was bonded to the outer wall of the elastomeric tube with another layer of elastomer. This was done by putting the mesh over the tube and dipping both into a basin of mixed prepolymer. When the tube was removed from the basin, the tube was blown with hot air while being rotated to evenly spread and cure the elastomer.

Finally, the ends of the actuator were closed by molding 1-2cm long elastomer plugs. The procedure for molding the plugs is shown in Fig. 4a. First, the tubing was put around a rod and the tubing was extended past the end of the rod by 2cm and mixed prepolymer was poured into the tubing. The plug was cured at 60°C for one hour. Next, an air supply line was inserted into the plugged end using a metal stylet. The remaining open end of the tube was dipped into a basin of mixed prepolymer to a depth of 1-2cm and cured at 60°C for 1 hour to form the second plug. During the dipping, the outer wall of the elastomer was covered with PTFE tape to prevent the outer walls from bonding to the prepolymer in the basin.

The finished actuators were up to 14cm long with 60%-70% of that length active (unplugged). The final outer diameter was about 8mm-14mm and the final wall thickness was about 1mm-2mm. Figure 4b shows some sealed actuators.

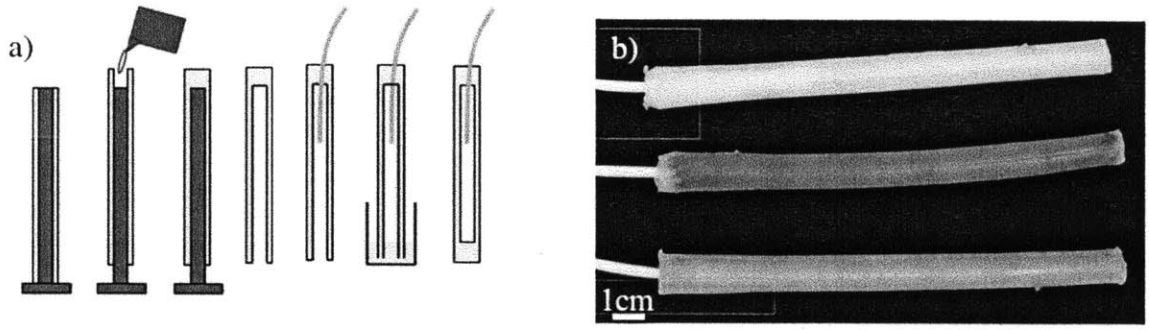

Figure 4.2: A) The procedure for sealing the ends of the actuator. B) The finished sealed actuators.

5 ACTUATOR EXPERIMENTAL CHARACTERIZATION

5.1 Experimental Procedure

The actuators were characterized to determine whether they provided the appropriate force, contraction, and rise time for use in DCC. Isometric contraction tests were conducted to determine output force as a function of internal pressure while actuator length was held constant, and constant pressure contraction tests were conducted to measure force as a function of contraction while pressure was held constant. The isometric contraction test was conducted quasistatically and dynamically. Anchor points were not used in the contraction testing on the tensile test machine so that the output force would not be limited by the strength of the anchors. Instead, the ends of the actuators were clamped in the jaws of the tensile test machine and the failure load of the anchor points were tested separately. Additionally, failure testing was conducted to determine the failure mode and pressure of the actuators.

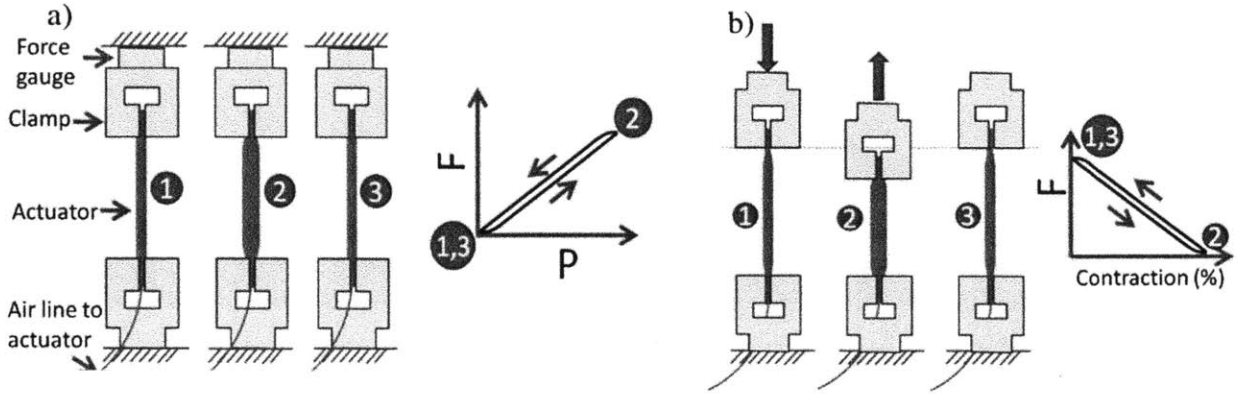

Figure 5.1: A schematic of the test procedure for the a) isometric contraction test and b) the constant pressure contraction test

For the isometric contraction test, the force output was measured using a 2kN load cell (±4N accuracy) and pressure was measured using a pressure transducer (±5 kPa accuracy) attached to the air supply line for the actuators. From these measurements, a force-pressure curve was generated. Figure 5a shows the test procedure. The pressure input was different in the quasistatic and dynamic testing. For the quasistatic response, the input pressure was slowly ($T \cong 60s$) ramped from 0 to 103kPa and back to 0 kPa using a pressure regulator. For the dynamic response a solenoid valve (2.4mm orifice, 4-16 milliseconds response time) was used to quickly deliver air at 103kPa from an accumulator (4.16L) to the actuators through about 1m of tubing (ID=3.2mm). A regulator was used to fill and continuously regulate the pressure in the accumulator.

For the constant pressure contraction test, the force and contraction were measured using a method previously used to characterize PAMs (Wehner et al., 2012). Figure 5b shows the experimental procedure. Tests were run at pressures of 34kPa, 69kPa, and 103 kPa and an

accumulator (4.16L) was again used to maintain constant pressure. The contraction was varied by moving the actuator ends while the reaction force at the supports was measured using a 2kN load cell (±4N accuracy). The actuator was allowed to contract until no load was measured at the supports (the "maximum contraction") and was then stretched back to the original length. Percent contraction was calculated by dividing displacement by the initial active length (10cm). The contraction frequency was near physiological rates. A normal resting heart rate ranges from about 0.7Hz-1.3Hz, whereas the actuators were tested at ram speeds consistent with about 0.5Hz contraction frequency.

Failure testing was also performed on the actuators. Pressure was delivered to each actuator using its air supply line and was slowly increased until failure. The tests were conducted with no load attached to the actuator. A pressure sensor (accuracy: ±5kPa) was used to measure the pressure during the test. The tests were filmed with a pressure sensor next to the muscle to enable confirmation of the pressure at the onset of failure. The experimental setup is shown in Figure 5.2.

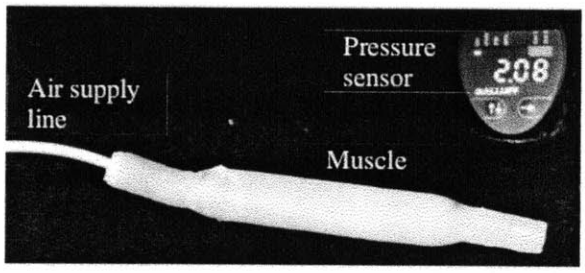

Figure 5.2: The experimental setup for failure testing. Pressure was ramped until failure while a video recorded the failure mode.

5.2 Experimental Results

5.2.1 Isometric Contraction Test Results

The force-pressure curves from the quasistatic isometric contraction test were used to measure the threshold pressure of the actuators and to examine the effects of initial braid angle and elastomeric material on the force output as a function of pressure. The low pressure region of the force-pressure curves was used to attempt to identify a threshold pressure. A typical force-pressure curve at low pressures is shown in Figure 5.3.

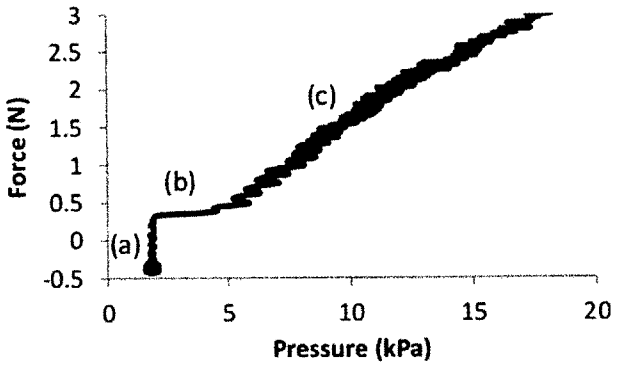

Figure 5.3: A typical force vs pressure curve for the pneumatic artificial muscles at low pressure

As the figure shows, the force-pressure curve is vertical in region (a) because an increase in force was measured before an increase in pressure was measured. In region (b), the pressure increase is detected and the pressure appears to increase without much change in force. After a pressure of about 5-7kPa, the measured force increases linearly with measured pressure (region (c)). This pattern was nearly identical across all actuators. Region (a) is clearly an artifact because force cannot be developed by the actuators without pressure. Since the force increase was detected before any pressure, no pressure threshold could be detected for any of the actuators, but factoring in the accuracy of the sensor (±5kPa), the threshold pressure of the

actuators can be said to be below 5kPa. This threshold pressure is an order of magnitude lower than those of McKibben air muscles tested in the literature(Chou & Hannaford, 1996; Daerden & Lefeber, 2002).

In addition to identifying the threshold pressure, the effect of the elastomeric material on force output was assessed by comparing the force-pressure curves of two actuators that differed only in elastomeric material. The curves of the actuators made from low stiffness (Ecoflex OO-30) and high stiffness (Elastosil M4601) elastomer are shown in Figure 5.4a. The slopes of the curves were similar between the muscles; the low stiffness actuator has a slope only 4% greater than the high stiffness actuator. The similarity between the curves was expected because deformation was prevented in this test, so almost no energy went to deforming the elastomer and therefore the different elasticities had little effect.

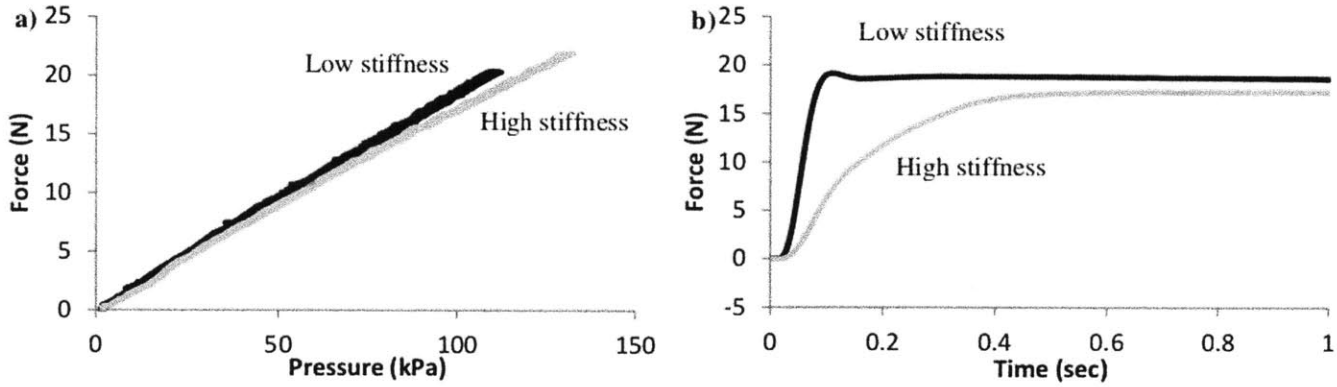

Figure 5.4: Isometric contraction curves for actuators made with elastomers of different stiffness. A) Quasistatic test results. B) Dynamic test results.

The dynamic responses of the two actuators are compared in Figure 5.4b. The actuator of the stiffer elastomer had a much longer rise time (0.28s vs. 0.05s). Based on the requirement of a rise time much less than 0.3 seconds, the actuator made of the softer elastomer contracted at a rate suitable for direct cardiac compression, but the actuator made of the stiffer elastomer did not.

The force-pressure curves from the isometric contraction test were also used to investigate the effects of initial braid angle on force output. The force-pressure curves of five artificial muscles that differ in initial braid angle are shown in Figure 5.5a. All of the actuators were made of the low stiffness elastomer. For the actuators with an increased initial diameter, the effect of an increased braid angle, which is decreasing force, dominated the effect of the increased diameter, which is increasing force. The slope of the force-pressure curve increased with decreasing initial braid angle, θi. All the actuators except the one with the highest θi were able to develop at least 10N of force at 100kPa. This is suitable for DCC because even a single actuator could deliver force in the desired 10-60N range at pressures of 100kPa.

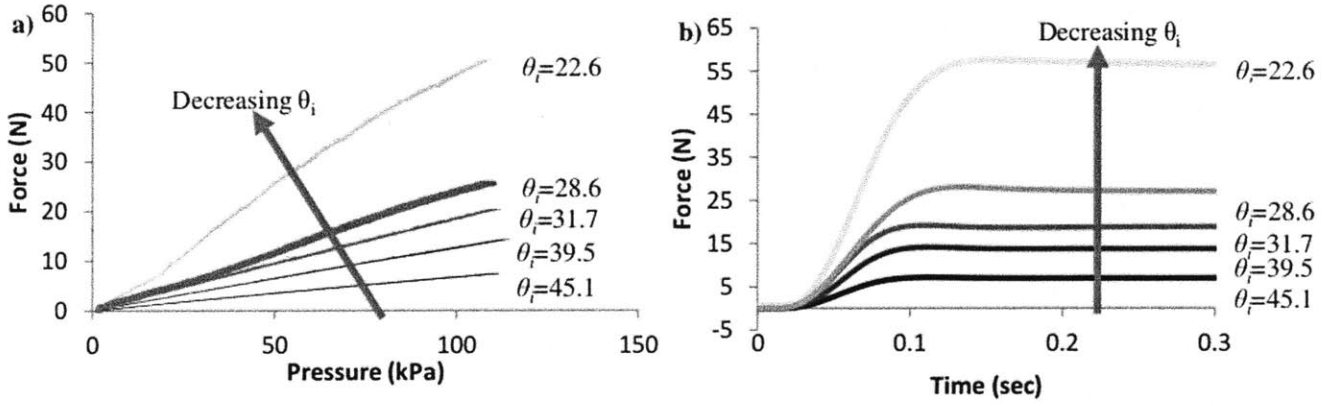

Figure 5.5: Isometric contraction curves for actuators with different initial braid angles. Quasistatic (a) and dynamic (b) test results.

The dynamic responses of the actuators are also compared in Figure 5.5b. All the actuators had a rise time of approximately 0.05s. This suggests that initial braid angle does not have much effect on rise time and that the contraction times are suitable for DCC according to our requirement.

5.2.2 Constant Pressure Contraction Results

The constant pressure test results were used to assess whether the actuators produced suitable contraction for DCC and to evaluate the effect of elastomeric material and initial mean braid angle on contraction. The effect of different elastomeric materials was measured by testing two actuators that differed in elastomer stiffness. Force-displacement curves of the actuators made of the low stiffness (Shore OO-30) and high stiffness (Shore A-28) elastomers are shown in Figure 5.6a. As predicted, the force decreased monotonically as contraction increased for both actuators. Also, the curves exhibited low hysteresis (~1 N high, and 1% wide) compared to other McKibben PAMs (Chou & Hannaford, 1996) possibly due to lower friction. The actuator made of the stiffer elastomer had a dramatically lower maximum contraction (10% vs 24%). Only the contraction of the low stiffness elastomer comes close to the functional requirement of roughly 25% contraction.

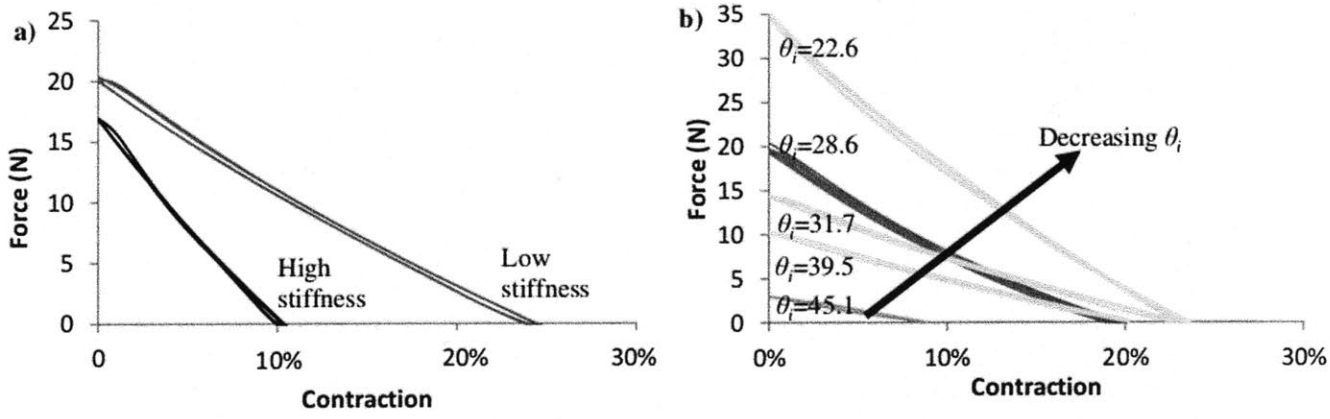

Figure 5.6: A) Effect of elastomeric material on force-contraction curve B) Effect of initial braid angle on force-contraction curve .

The force-displacement curves of five artificial muscles that differed in braid angle are shown in Figure 5.6b. All of the curves shown in the figure were taken at a pressure of 69 kPa. Each of the curves is monotonically decreasing and roughly linear. Again, the hysteresis was small (~1N high and 1% wide). The maximum contraction and maximum force tended to increase with a decreasing initial mean braid angle, but it seems that the effect on maximum contraction was diminishing after θ_i=39.5°.

The actuator with θ_i=28.6° was an outlier because it had a lower maximum contraction than two actuators with a higher braid angle. This may be explained by the difference in mesh properties besides the braid angle, namely the weave density. Davis showed that higher fiber density caused a lower maximum contraction (Davis, 2006). The two actuators with the lowest braid angle (θ_i=28.6°, θ_i=22.6°) had a higher weave density than the rest of the actuators, which had the same weave density.

In all of the actuators, a trade-off between force and contraction is apparent. It is difficult for the actuators to produce both high force and high contraction at once because force decreases with increasing contraction. However, force can be increased by adding more actuators in parallel which might enable more force to be sacrificed for contraction.

The actuators with lower initial mean braid angles were able to deliver greater force and contraction, so the most promising design seems to be one with the lowest possible initial mean braid angle. However, there is a lower limit to the initial mean braid angle because radial expansion increases with decreasing initial mean braid angle and space in the pleural cavity is limited. The actuators developed here undergo a diameter increase of about 1cm during contraction. This radial expansion is not considered to be large enough to be a problem for DCC,

but in the future, the maximum allowable radial expansion should be determined to define the lowest feasible initial mean braid angle.

5.2.3 Failure Test Results

The first failure mode of the actuators made of the less stiff elastomer and θ_i=31.7° was that the air supply line slipped out. The line was ejected at 138kPa - 228kPa for three specimens made of the softer elastomer (Ecoflex OO-30) with θ_i=31.7°. The air supply line was not ejected for the four actuators made of high stiffness elastomer (Wacker M4601), unreinforced ends, and θi=31.7°, but the plug opposite the air supply line failed. Failure occurred at 270kPa, 600kPa, and 720kPa. All of these ruptures pressures are significantly higher than the operating pressure of 100kPa. The variation in rupture pressure was high, especially for the stiffer actuators, so testing of a larger sample size is needed to identify the factors that cause this variation.

6 INTEGRATED CARDIAC COMPRESSION DEVICE

Two integrated prototypes were made out of the PAMs for experimental validation in an animal model. One design was made by molding the actuators into an elastomeric band to fit around the heart. The second prototype was made by attaching the actuators to a mesh that could be sutured to a patient's heart during surgical implantation.

6.1 Molded Elastomeric Band

6.1.1 Design

The goal of the elastomeric band design was to embed actuators in an elastomeric structure flexible enough to fit securely over hearts of different sizes. The band design consisted of two active elastomeric sheets with embedded PAMs, one for each side of the heart, and two passive elastomeric ribbons which connected the two sheets to form a band. The actuators embedded in the active sheet were to be connected to each other with less elastomer and softer elastomer relative to elastomeric sheets with embedded PAMs in the literature (Chen, Yin, Liu, & Leng, 2011) because increasing the volume and stiffness of the elastomer connections increases the amount of energy needed for contraction of the sheet. The connections between actuators in the design were only 2mm thick so that nearly as much contraction could be obtained from the sheet of actuators as for an individual actuator not embedded in a sheet. The elastomeric sheet was also designed so that each actuator could be contracted independently without significantly affecting the contraction of adjacent actuators. This was accomplished by adding adequate spacing between actuators embedded in the sheet (1cm). In addition, the sheet was designed to be molded in as few steps as possible to reduce the number of weak bond interfaces. After a part is molded once, cross linking is already underway in the elastomer and subsequent bonds are weaker than the bonds made at the start of cross linking. The mold for the active sheet design is shown in Figure 6.1.

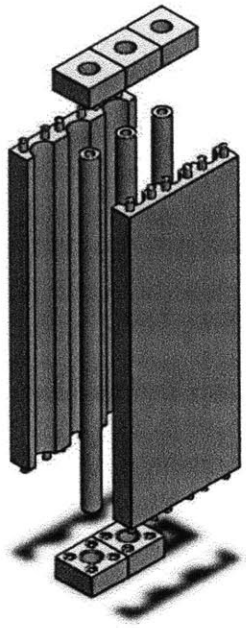

Figure 6.1: Mold design for elastomeric band

The two elastomeric ribbons that connected the two active sheets were intended to provide the compliance needed to allow the device to fit hearts of different sizes without slack or excessive tightness. One of the two ribbons was designed to also act as a hub and a strain relief for the tubing from the actuators. The passive elastomeric ribbon and the active elastomeric sheet were designed to have the same cross section so that the ends of each could be joined together smoothly.

6.1.2 Fabrication and Evaluation

For the molded elastomeric band prototype, the softer elastomer (Ecoflex OO-30) was used to create the prototype because of the advantages of using a soft elastomer shown in Section

5.2.2. The active sheets with the embedded actuators were each cast in one step so that the actuators within each sheet would be firmly bonded to each other. Meshes with $\theta_i = 31.7$ were placed on the three rods (8mm OD). The mold was filled with elastomer and the rods were inserted into the holes (12mm ID) in the mold and were held concentric using alignment holes on the ends of the mold. The mold was cured for an hour at 60 C. When the sheet was removed from the mold, the meshes were embedded on the inner diameter of the channels created by the rod. The ends of each channel were sealed with elastomer plugs and air supply lines were added as described in section 4.2. After being plugged, the channels functioned like Mckibben actuators since their expansion was constrained by the meshes embedded in them. Figure 6.2 shows one of the finished active sheets contracting.

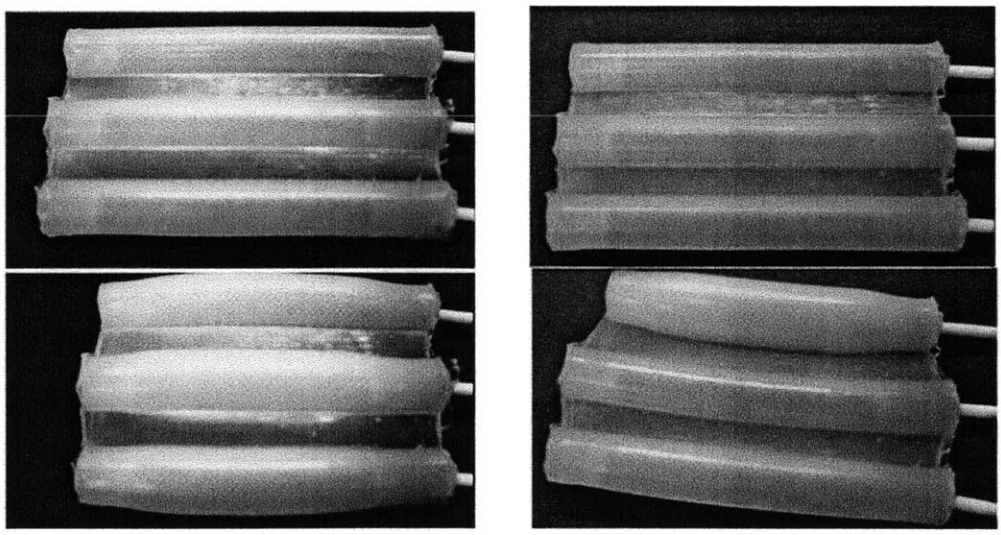

Figure 6.2: A sheet of PAM actuators before contraction (top) and after full contraction (bottom left) and after independent contraction of only the top actuator (bottom right)

The drawback of this molding method is that since the mesh is on the inner diameter of the channels, the mesh may not be encapsulated by elastomer on both sides. Specifically, the side of the mesh that was against the rod during molding is not bonded to elastomer. This can cause

delamination to occur between the mesh and the channel, causing failure of the actuators. For this reason the operating pressure of the active sheet was limited to 67kPa.

Also, actuators made using this method are prone to air leakage. When the mesh is embedded in the wall of the tubing and the mesh is about as thick as the wall of the tubing, the mesh fibers create small channels through the elastomer that air can travel through (Figure 12). The mesh with $\theta_i = 31.7$ was best for molding the active sheet because it was thinner and therefore created sheets that were more air tight than the meshes with lower initial braid angles.

The fabrication process for making the elastomeric band prototype from the sheets is shown in Figure 6.3. The two contractile sheets were connected together with one elastomeric ribbon (Figure 6.3b), and were then joined end to end using another elastomeric ribbon to make the finished device (Figure 6.3c). The air supply lines were routed through the second elastomeric ribbon.

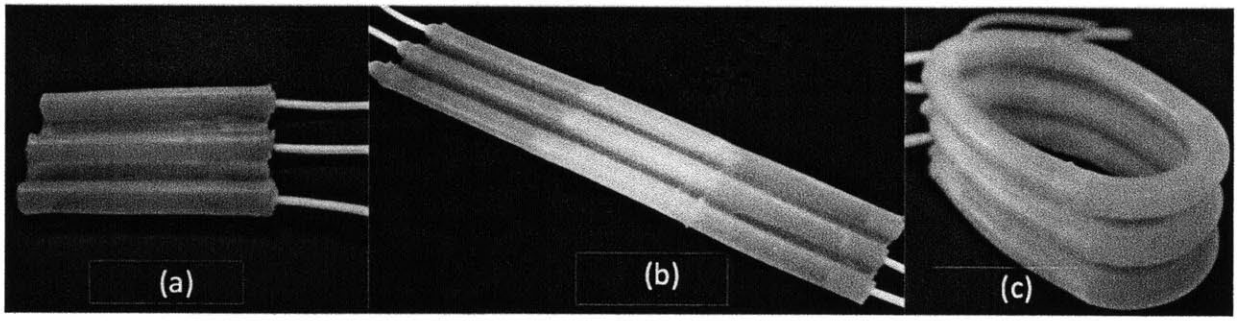

Figure 6.3: The fabrication procedure for the molded elastomeric band.

To evaluate the performance of the device, the finished prototype was actuated at 10 psi around a heart model approximately 100 times at 1Hz. The device was able to stretch to tightly fit the heart model used for the evaluation. All the actuators contracted successfully with no signs

of delamination between the mesh and the elastomer of the actuators and the air supply tubing remained in place.

One shortcoming of the prototype was that multiple cracks were initiated and propagated at the interfaces between the active sheets and the elastomeric ribbons after repeated contraction and handling of the device. This failure is caused because all the tension generated by the actuators must be carried by that interface. In the future, this failure may be prevented by bonding the sheets more quickly, when less cross linking has occurred. Another potential solution is to design an interlocking interface rather than a straight one. This would increase the surface area of the bond and attach in such a way that the interface is loaded not entirely in tension, because bonded interfaces are better at resisting shear and compression.

Another shortcoming was that the band connecting the two sheets was perhaps overly compliant. It seemed that much of the energy and contraction delivered by the actuators was used to stretch the band rather than actuate the heart model. This can be addressed by simply changing the stiffness of the elastomer used for the ribbons, or by reducing their length to increase the stiffness. Decreasing the length of the ribbons would also allow the length of the active sheets to be increased.

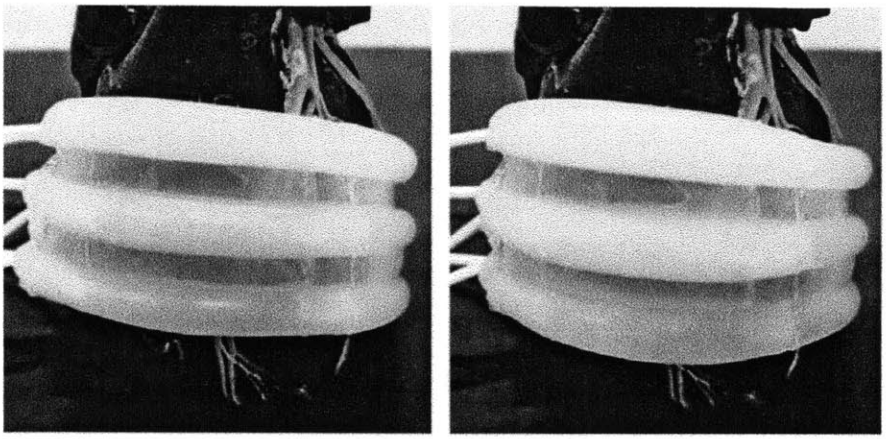

(a) (b)

Figure 6.4: The integrated cardiac compression device was actuated around a model heart. (a) Before inflation air muscles are in the neutral position. (b) After inflation air muscles are in contracted position

6.2 Mesh-based prototype

6.2.1 Design

The second prototype was designed to be based on a mesh and to maximize power delivery to the heart. The prototype was based on a mesh fabric because cardiac surgeons are familiar with suturing to the heart. Also, the mesh based prototype gives the surgeon the flexibility to resize the device at the time of surgery. The mesh used in the prototype was chosen to be similar to a mesh that was designed to be sutured around the heart (CorCap, Acorn Cardiovascular, Inc.) and was used in human trials.

To maximize power delivery the actuators parameters were chosen for maximum force and displacement, the active (actuated) area of the device was maximized, and the operating pressure was increased. To create actuators with high contraction and force generation, the actuators were made of the softer elastomer and had the lowest initial braid angle because of the results in section 5.2.2. To further increase power output, the number of actuators on the mesh was

maximized (based on the average size of sheep hearts). Five rows of actuators were used (11 total) and they were placed as tightly together as possible. Anchor points had to be added to the actuators to bond them to the mesh. Multiple anchor point designs were evaluated and a design that used fishing line to tie actuators to nodes of the mesh was chosen because it was best for rapid prototyping since it was easily reversible and allowed for repositioning of the actuators. In addition to increasing active area, the operating pressure was raised to 100 kPa from the 67kPa used in the previous prototype. In order to accommodate the higher pressure without leaking or having the air supply line disconnect, the plugs were reinforced with the stiffer elastomer.

6.2.2 Fabrication

The actuators for the mesh-based prototype were fabricated using the procedure in Chapter 4. Because of the shorter plugs and high operating pressure, the ends of the actuators had to be reinforced with 5mm plugs of a stiffer elastomer (Elastosil M4601) to prevent air leaks and hold the air supply line in. The procedure for reinforcing the ends is shown in Figure 6.5. First the reinforcing elastomer was injected into the bottom end of an actuator and the actuator cured in an upright position for an hour at 60 C. Next the actuator was flipped and the procedure was repeated for the new bottom end. Finally, the air supply line was inserted through one of the reinforced ends.

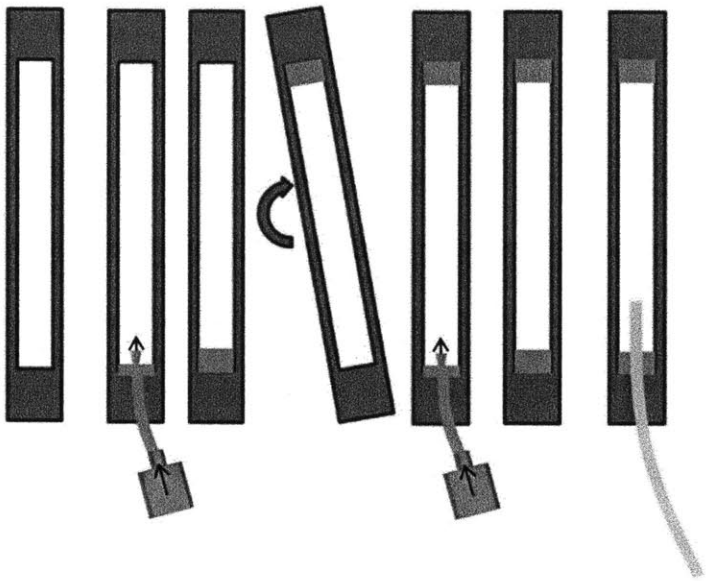

Figure 6.5: The process for reinforcing the actuator ends. Stiffer elastomer was injected into each end of the actuators.

Attachment between the actuators and the mesh was achieved by adding anchor points to the actuators and then fastening those points to the mesh. A load carrying line was tied directly to the outer diameter of the plugged ends. This attachment method can withstand up to about 15N of axial force based on failure testing conducted on the anchor points that involved repeatedly actuating (~10 times) at a pressure of roughly 70kPa with a load applied to the anchor points. The load was increased by 0.5kgf until failure or 3kg was reached. Figure 6.6 shows the experimental setup.

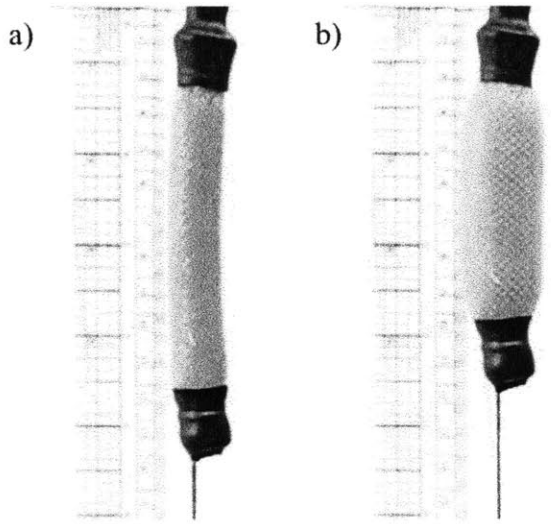

Figure 6.6: A photograph of the experimental setup for the anchor point failure test. The actuators were repeatedly actuated at increasing loads. A) The actuator at rest B) The contracted actuator

The finished actuators were attached to the mesh fabric. The mesh was cut into a shape that when connected end to end would form a frustrum that was sized for a large sheep heart. The excess mesh on the ends can be cut to reduce the size of the mesh so that it can fit around smaller hearts.

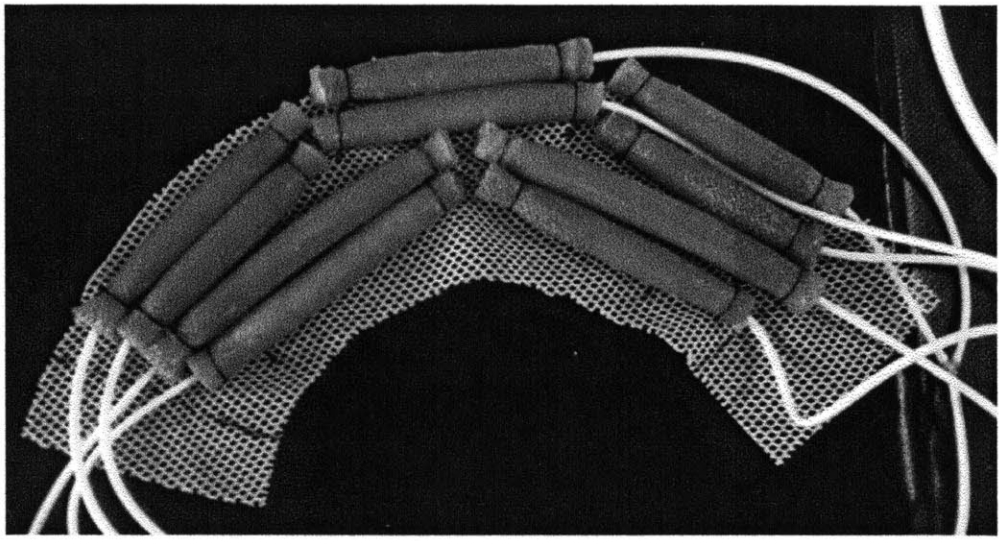

Figure 6.7: The mesh-based prototype

6.3 Control System

The extracardiac compression device required a control system and portable pressure source for animal testing. Figure 6.8 shows a diagram of the setup. A portable air compressor (DeWALT Heavy-Duty 4.5 Gallon, 200 PSI) is used to supply air pressure. The compressor has a built in accumulator that helps smooth output pressure. A pressure regulator set to 60 – 100 kPa is used to down regulate the supply pressure. A three way solenoid valve allows the device to be alternatively pressurized and vented to the atmosphere. The solenoid valve is controlled by a microcontroller. The microcontroller sends a square wave between low (0 V) and high (5 V) at an average frequency of about 70 Hz (30% duty cycle) to a power MOSFET, which connects the power supply to the solenoid on the high signal. The duty cycle is set so that 30% of the cycle will be spent in contraction and 70% in expansion, similar to a natural heart. The signal from the pressure gauge microcontroller is recorded by the microcontroller.

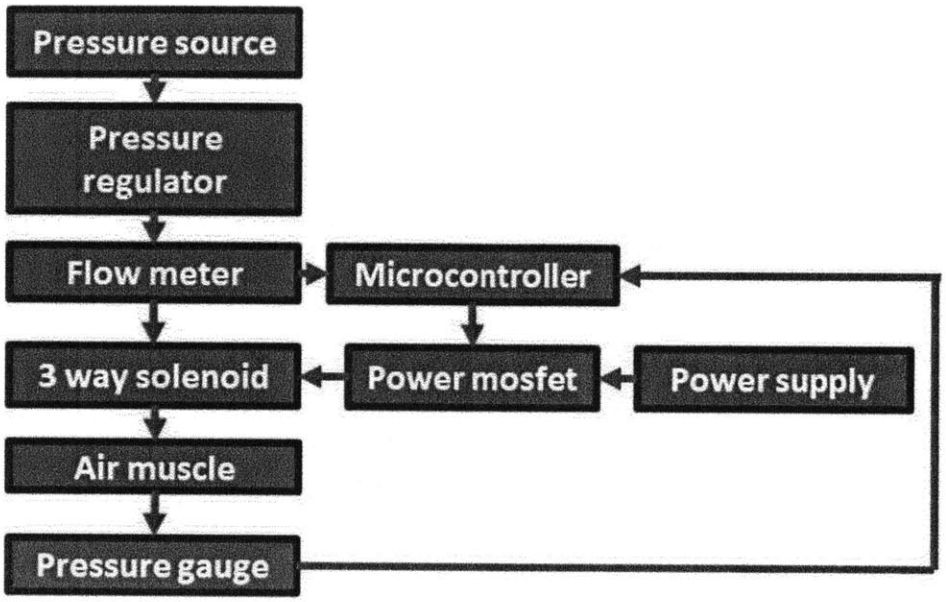

Figure 6.8: Control system for testing the extracardiac compression device

7 CONCLUSION

Our experimental data showed that the fully soft pneumatic artificial muscles (PAMs) developed here have the ability to deliver suitable forces, contractions, and rise times for direct cardiac compression (DCC) in the pressure range of 0-100kPa. The actuators developed here also have threshold pressures significantly lower than traditional McKibben PAMs [1] which enables more precise control of force and displacement at low pressures.

The experimental results indicate that elastomeric material and initial mean braid angle greatly affect performance of the actuators. A softer elastomer enabled greater contraction and a much faster response time while a lower initial mean braid angle increased force output and maximum contraction. These results suggest that a DCC device powered by these actuators is feasible. Two DCC devices made from the actuators were designed and fabricated for an acute animal study. The results of the animal study may determine whether such a DCC device is viable.

8 APPENDIX A

The design of the mold used to create the actuators

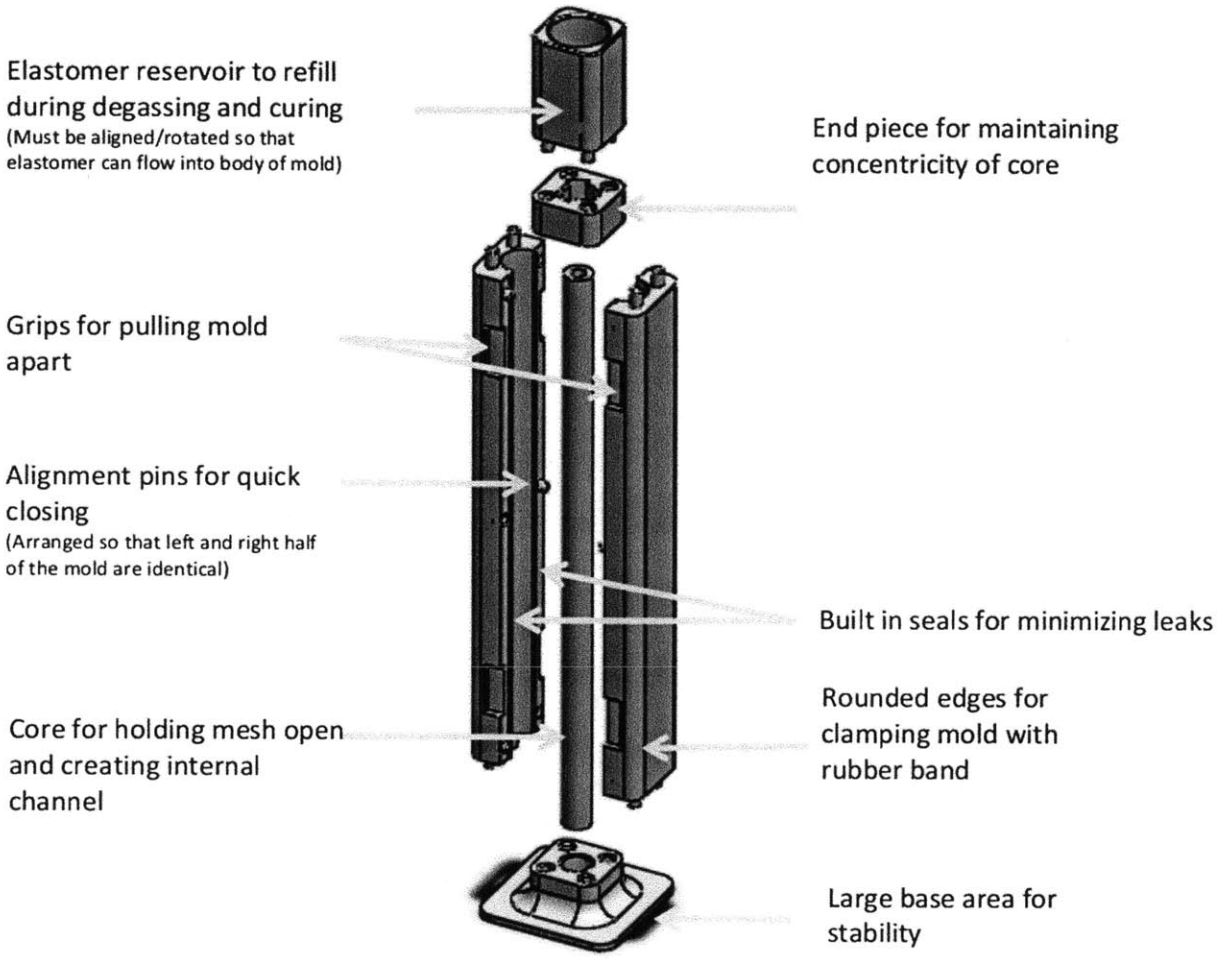

9 REFERENCES

Alazmani, A., Keeling, D. G., Walker, P. G., Abbas, S. K., Jaber, O., Watterson, K., & Levesley, M. C. (2012). Introducing a Hardware-in-the-Loop Simulation of the Cardiovascular System. *Heart*.

Andrikopoulos, G., Nikolakopoulos, G., & Manesis, S. (2011). A Survey on Applications of Pneumatic Artificial Muscles. *Proceeding of the 10th Mediterranean Conference on Control Automation (MED)*, 1439–1446. doi:10.1109/MED.2011.5982983

Anstadt, M. P., Perez-Tamayo, R. A., Banit, D. M., Walthall, H. P., Cothran, R. L., Abdel-Aleem, S., Anstadt, G. L., et al. (n.d.). Myocardial tolerance to mechanical actuation is affected by biomaterial characteristics. *ASAIO Journal*, *40*(3), M329–34. Retrieved from http://www.ncbi.nlm.nih.gov/pubmed/8555534

Carrington, R., & Huang, Y. (2003). Direct compression of the failing heart reestablishes maximal mechanical efficiency. *The Annals of Thoracic Surgery*, 190–196. Retrieved from http://www.sciencedirect.com/science/article/pii/S0003497502041668

Chen, Y., Yin, W., Liu, Y., & Leng, J. (2011). Structural design and analysis of morphing skin embedded with pneumatic muscle fibers. *Smart Materials and Structures*, *20*(8), 085033. doi:10.1088/0964-1726/20/8/085033

Chou, C., & Hannaford, B. (1994). Static and dynamic characteristics of McKibben pneumatic artificial muscles. *IEEE Conference on Robotics and Automation*. Retrieved from http://ieeexplore.ieee.org/xpls/abs_all.jsp?arnumber=350977

Chou, C., & Hannaford, B. (1996). Measurement and modeling of McKibben pneumatic artificial muscles. *IEEE Conference on Robotics and Automation*, *12*(1), 90–102. Retrieved from http://ieeexplore.ieee.org/xpls/abs_all.jsp?arnumber=481753

Daerden, F., & Lefeber, D. (2002). Pneumatic artificial muscles: actuators for robotics and automation. *European Journal of Mechanical and Environmental Engineering*. Retrieved from http://pdf.aminer.org/000/351/318/pneumatic_muscle_actuator_technology_a_light_weight_power_system_for.pdf

Davis, S. (2006). Braid Effects on Contractile Range and Friction Modeling in Pneumatic Muscle Actuators. *The International Journal of Robotics Research*, *25*(4), 359–369. doi:10.1177/0278364906063227

Horn, B., & Kuipers, M. (1988). Strength and stiffness of a reinforced flexible hose. *Applied scientific research*, *281*, 251–281. Retrieved from http://www.springerlink.com/index/l181h7709tg3p6m1.pdf

Huang, Y., & Hunyor, S. (2004). Implantable direct cardiac compression device and system. *US Patent App. 10/567,520*. Retrieved from http://www.google.com/patents?hl=en&lr=&vid=USPATAPP10567520&id=z2eiAAAAEBAJ&oi=fnd&dq=Implantable+direct+cardiac+compression+device+and+system&printsec=abstract

Klute, G. K., Czerniecki, J. M., & Hannaford, B. (1999). McKibben artificial muscles: pneumatic actuators with biomechanical intelligence. *1999 IEEE/ASME International Conference on Advanced Intelligent Mechatronics*, 221–226. doi:10.1109/AIM.1999.803170

Kung, R. T., & Rosenberg, M. (1999). Heart booster: a pericardial support device. *The Annals of Thoracic Surgery*, *68*(2), 764–7. Retrieved from http://www.ncbi.nlm.nih.gov/pubmed/10475485

Mau, J., Menzie, S., Huang, Y., Ward, M., & Hunyor, S. (2011). Nonsurround, nonuniform, biventricular-capable direct cardiac compression provides Frank-Starling recruitment independent of left ventricular septal damage. *The Journal of Thoracic and Cardiovascular Surgery*, *142*(1), 209–15. doi:10.1016/j.jtcvs.2010.05.057

Melvin, D. (2006). Heart wall actuation system for the natural heart with shape limiting elements. *US Patent 6,988,982*. Retrieved from http://patentscope.wipo.int/search/en/WO2004016159

Ming, Y., Meiling, Z., Richardson, R. C., Levesley, M. C., Walker, P. G., & Watterson, K. (2005). Design and evaluation of linear ultrasonic motors for a cardiac compression assist device. *Sensors and Actuators A: Physical*, *119*(1), 214–220. doi:10.1016/j.sna.2004.09.005

Moreno, M. R., Biswas, S., Harrison, L. D., Pernelle, G., Miller, M. W., Fossum, T. W., Nelson, D. a., et al. (2011a). Assessment of Minimally Invasive Device That Provides Simultaneous Adjustable Cardiac Support and Active Synchronous Assist in an Acute Heart Failure Model. *J. Med. Devices*, *5*(4), 041008. doi:10.1115/1.4004652

Moreno, M. R., Biswas, S., Harrison, L. D., Pernelle, G., Miller, M. W., Fossum, T. W., Nelson, D. a., et al. (2011b). Development of a Non-Blood Contacting Cardiac Assist and Support Device: An In Vivo Proof of Concept Study. *J. Med. Devices*, *5*(4), 041007. doi:10.1115/1.4005281

Mosterd, a, Hoes, a W., De Bruyne, M. C., Deckers, J. W., Linker, D. T., Hofman, A., & Grobbee, D. E. (1999). Prevalence of heart failure and left ventricular dysfunction in the general population; The Rotterdam Study. *European Heart Journal*, *20*(6), 447–55. Retrieved from http://www.ncbi.nlm.nih.gov/pubmed/10213348

Mosterd, A., & Hoes, A. W. (2007). Clinical epidemiology of heart failure. *Heart (British Cardiac Society)*, *93*(9), 1137–46. doi:10.1136/hrt.2003.025270

Oberman, a., Myers, a. R., Karunas, T. M., & Epstein, F. H. (1967). Heart Size of Adults in a Natural Population-Tecumseh, Michigan: Variation by Sex, Age, Height, and Weight. *Circulation*, *35*(4), 724–733. doi:10.1161/01.CIR.35.4.724

Oz, M. C., Artrip, J. H., & Burkhoff, D. (2002). Direct cardiac compression devices. *The Journal of Heart and Lung Transplantation*, *21*(10), 1049–55. Retrieved from http://www.ncbi.nlm.nih.gov/pubmed/12398868

Schulte, H. (1961). The characteristics of the McKibben artificial muscle. *The Application of External Power in Prosthetics and Orthotics*, 94–115. Retrieved from http://scholar.google.com/scholar?hl=en&btnG=Search&q=intitle:The+characteristics+of+the+McKibben+artificial+muscle#0

Shahinpoor, M. (2010). A Review of Patents on Implantable Heart-Compression / Assist Devices and Systems. *Recent Patents on Biomedical Engineering*, 54–71.

Shahinpoor, M., & Kim, K. (2001). Design, development, and testing of a multifingered heart compression/assist device equipped with IPMC artificial muscles. *SPIE's 8th Annual International Symposium on Smart Structures and Materials*, *4329*, 411–420. Retrieved from http://proceedings.spiedigitallibrary.org/proceeding.aspx?articleid=1279415

Shiraishi, Y., Yambe, T., Sekine, K., Saijo, Y., Wang, Q., & Liu, H. (2005). Development of an Artificial Myocardium using a Covalent Shape-memory Alloy Fiber and its Cardiovascular

Diagnostic Response. *Proceedings of the 27th Annual Conference of the IEEE Engineering in Medicine and Biology*, *1*, 406–8. doi:10.1109/IEMBS.2005.1616431

Tondu, B. (2012). Modelling of the McKibben artificial muscle: A review. *Journal of Intelligent Material Systems and Structures*, *23*(3), 225–253. doi:10.1177/1045389X11435435

Trumble, D. R., Park, C. S., & Magovern, J. a. (1999). Copulsation Balloon for Right Ventricular Assistance : Preliminary Trials. *Circulation*, *99*(21), 2815–2818. doi:10.1161/01.CIR.99.21.2815

Vasan, R., Benjamin, E., & Levy, D. (1995). Prevalence, clinical features and prognosis of diastolic heart failure: an epidemiologic perspective. *Journal of the American College of ...*, *26*(7), 1565–74. doi:10.1016/0735-1097(95)00381-9

Walker, P. G., Keeling, D. G., Levesley, M. C., Hanson, B., Watterson, K., & Ipereni, C. (n.d.). Do We Need Active Relaxation in Artificial Cardiac Muscles? *Engineering In Medicine And Biology*, *1*, 2–4.

Wehner, M., Park, Y.-L., Walsh, C., Nagpal, R., Wood, R. J., Moore, T., & Goldfield, E. (2012). Experimental characterization of components for active soft orthotics. *Proc. IEEE Int. Conf. Biomed. Rob. Biomechatron.*, 1586–1592. doi:10.1109/BioRob.2012.6290903

Woods, B. K., Gentry, M. F., Kothera, C. S., & Wereley, N. M. (2012). Fatigue life testing of swaged pneumatic artificial muscles as actuators for aerospace applications. *Journal of Intelligent Material Systems and Structures*, *23*(3), 327–343. doi:10.1177/1045389X11433495